Visible-light photocatalysis of PDI nanowires enhanced by plasmonic effect of the gold nanoparticles

Hong Miao[a], Jun Yang[a], Yunxia Wei[b], Wenlu Li[a], Yongfa Zhu[a,*]

[a] Department of Chemistry, Tsinghua University, Beijing 100084, PR China
[b] College of Chemistry and Chemical Engineering, Lanzhou City University, Lanzhou 730070, PR China

ABSTRACT

PDI molecules catalysts had shown much great advantages such as optical properties and chemical electronic tunability, rich elements of resources and structural diversity. These organic materials are considered as a promising route to mitigate water pollution or other environmental problems. So, many researchers have conduct related research in the past few decades. Otherwise, surface plasmon resonance (SPR) effect of the AuNPs could promote the absorption of visible light effectively. Herein, SPR-supported visible-light-responsive photocatalyst of PDI@AuNPs were prepared through the electrostatic adsorption. The results show that the PDI@AuNPs composite appeared higher visible light degradation rate (k) towards the phenol, which is 1.7 times than the PDI nanowires. The highly photocatalytic activity of the PDI@AuNPs could own to the surface plasmon resonance (SPR) of AuNPs. Specifically, SPR effect of the AuNPs and the RET process between AuNPs and PDI could be beneficial for utilizing the visible light. Thus, the visible light utilization of PDI@AuNPs is higher than the PDI nanowires. Meanwhile, the ability of electrons and holes separation are greatly improved by the lower Fermi level of Au, which is favorable for the efficient transfer of the photo-excited electron-hole pairs. Overall, the system of the PDI@AuNPs composite is responsible for the highly efficient photocatalytic degradation of pollutants. What's more, the PDI@AuNPs composite simultaneously exhibits great stability and cycle utilization than the pure PDI.

1. Introduction

In recent years, photocatalyst have attracted great interest due to the use of solar energy for environmental protection applications (water purification, air purification, antibacterial sterilization, antifouling dust). Titania-based catalyst has proven to be an excellent photocatalyst material under UV light exposure [1,2] and has been extensively investigated. Furthermore, it has appeared many advantages such as the low cost, high activity and stability. So it was regard as one of the most photoactive inorganic semiconductor catalysts. But its gap width ($\sim 3.2\,eV$) limited the photocatalytic performance in visible light [3]. Therefore, in order to increasing the photocatalytic performance, the crystal phase of TiO_2 has been regulated by various methods and synthesis technology. [4–13] In addition to the TiO_2 or other inorganic, many researchers have been working at developing new visible light organic materials catalyst in recent years.

Organic materials have exhibited great advantages of optical properties and chemical electronic tunability, rich elements of resources and structural diversity compared with the inorganic materials. Many

researchers have conduct related research in the past few decades. Molecule self–assembly methods have been studied to tailor the surface properties of the catalyst, [14] non-covalent supramolecular system composed of pure organic molecules alone as a photocatalyst has been reported recently, which has shown wide visible light response. These methods have been put forward to increase the photocatalytic activity. PDI supramolecular organic photocatalyst formed from the PDI molecules is a special n-type organic semiconductor material. It exhibits high electron affinity and charge carrier mobility [15–19]. Thus, it could be useful for the visible light oxidation of water and organic pollutants degradation.

On the other hand, the surface plasmon resonance (SPR) of the metal had been studied deeply, which has been employed to improve the efficiency of photocatalysts under the visible light. According to the reports, the SPR effect increases the solar conversion efficiency mainly contains three process, (i) increasing light scattering, (ii) enlarging the visible light absorption, and (iii) the plasmonic energy from the metal could be transferred to the semiconductor. [20,21] Thus, the photocatalytic activity of the semiconductors could be enhanced by the
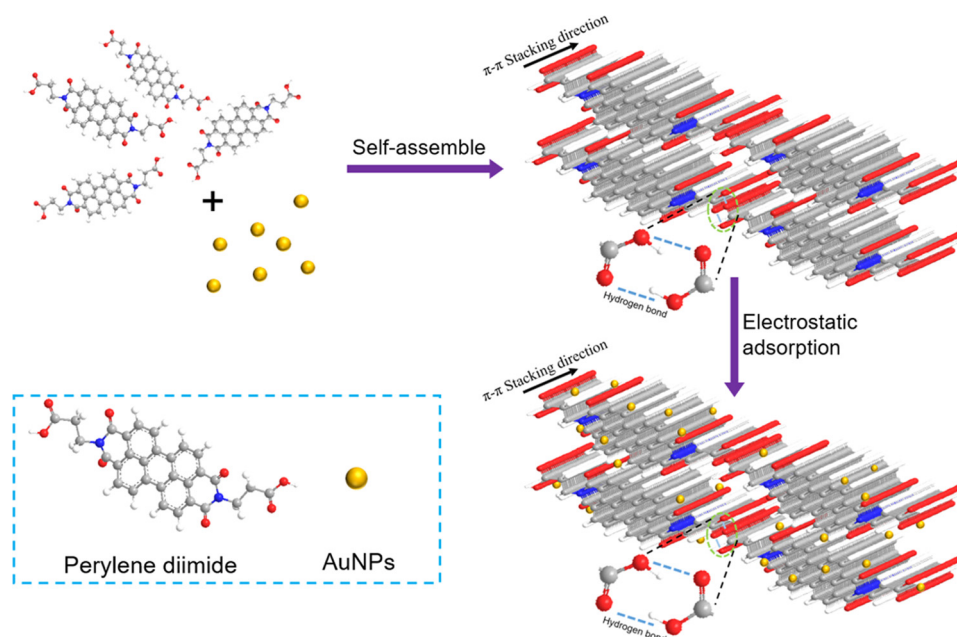
Scheme 1. Schematic illustration of synthesizing self-assembled PDI and compositing with AuNPs.

deposition of plasmonic gold nanoparticles (AuNPs), which could be better used for the organic compound oxidation and water splitting [22–30]. Practically speaking, the concentrated energy from the AuNPs is transferred to the semiconductor through process (iii), which could be contributed to increase the carriers separation of the semiconductor. Thus, the SPR-supported system could offer a new opportunity to increase the electron-hole pair separation and improve the photocatalytic activity. It is studied as the resonance energy transfer (RET) process could enhance the create carriers in the semiconductor [20,21].

Hereby, we reported the photocatalytic oxidation of phenol by a SPR-supported visible light responsive the photocatalyst of self-assembled PDI (PDI@AuNPs) (Scheme 1). The AuNPs were deposited on the surface of the self-assembled PDI through the electrostatic adsorption process. Therefore, the PDI@AuNPs has shown a satisfactory photocatalytic activity under visible light irradiation ($\lambda > 420$ nm). Compared with the PDI nanowire, the PDI@AuNPs composite appeared a higher carrier separation efficiency, which is in favor of increasing the highly efficient photocatalytic degradation of pollutants.

2. Experimental section

2.1. Synthesis of PDI@AuNPs composites

The perylene diimide (PDI) were synthesized by the previous work. [18,31] Firstly, 1.376 g (3.507 mM) of perylene-34,910-tetracarboxylic dianhydride, 18 g of imidazole and 2.5 g (28.06 mM) of 3-aminopropionic acid (all of them were supplied by the Aldrich) were heated at 110 °C for 4 h under the protection of argon in a three–necked flask. Next the reaction mixture was dispersed in 300 mL of HCl (2 M) and 100 mL ethanol stirred overnight. Then, the final red solid was washed to neutral with distilled water and filtrated through a 0.22 μm membrane filter. Finally, the collected red solid was dried under vacuum at 60 °C in oven and powdered for further applications.

The sodium citrate reduction method was used to prepare the 13 nm AuNPs. [32] All glassware were cleaned by the aqua regia (HCl/HNO$_3$, 3:1) and then rinsed with H$_2$O. First, 100 mL of HAuCl$_4$ (1 mM) solution was heated to boiling with vigorous stirring and then 10 mL of trisodium citrate (38 mM) solution was added under stirring together. The mixture solution was continued boiling for an additional 15 min until the color of the AuNPs changed from light yellow to red. Finally, AuNPs

were centrifuged about 10 min at 12,000 rpm and redispersed by the water to obtianed the final AuNPs (1.86 mg/mL). The prepared gold nanoparticle were stored at 4 °C.

Preparation of PDI@AuNPs composites. Firstly, 0.276 g of N, N'-bis (propionic acid)–phenyl–34,910–tetracarboxylic acid diimide was dispersed in 100 mL water under sonication about 30 min. Next, 417 μL of triethylamine solution was added to the PDI stock solution with constantly stirring. Then, 15 mL of AuNPs (1.86 mg/mL) were added to the stock solution with vigorous stirring about 30 min. Followed by adding 13 mL of HCl (4 M) and continue stirring for 3 h, then ultrasound 30 min. Finally, the product was centrifuged and washed to neutral. Finally, the solid was collected and dried under vacuum at 60 °C and powdered for further use.

2.2. Characterization of photocatalyst materials

The lattice plane stripe of PDI@AuNPs were observed by the high-resolution transmission electron microscopy (HRTEM, JEM 2010 F). The morphology of the materials prepared here were studied by the transmission electron microscope (TEM, Hitachi HT7700) and the scanning electron microsopy (FE-SEM, Hitachi SU-8010). UV–vis spectrophotometer (Hitachi U-3010) were used to obtain the UV–vis diffuse reflection spectra (DRS) of the samples. The reflectance standard was BaSO$_4$. X-ray photoelectron spectroscopy (XPS ULVAC-PHI, Quantera) were used to analyse the elemental of the PDI@AuNPs nanomaterials. Zeta potentials of the PDI nanowire, AuNPs and PDI@AuNPs were measured with a Horiba SZ-100 Nano Particle analyzer. Fluorescence spectra of the samples were record on Perkin-Elmer LS55 spectrophotometer. The FT-IR spectra of the PDI nanowire and PDI@AuNPs were measured by a Bruker V70 spectrometer. The electrochemical impedance and photocurrent response were measured by the electrochemical workstations (CHI-660E, China). The JES-FA200 EPR Spectrometer paramagnetic resonance spectrometer was used to detect the mainly active species. The 500 W xenon lamp with a 420 nm cutoff filter was used to provide the visible light (Institute for Electric Light Sources, Beijing).

2.3. Photocatalytic experiments

The degradation of the phenol solution experiments were used to

evaluate the photocatalytic activity of the prepared PDI@AuNPs composite materials under visible light. 25 mg PDI@AuNPs composite materials powder and 50 mL of phenol (5 ppm) were added in a quartz tube reactor before the photodegradation reaction. 500 W xenon lamp with a bandpass filter (450, 500, 520, 550, 600 ± 15 nm) or cutoff filter (> 420 nm) were applied to offer the visible light. First, the suspension solution was ultrasonically dispersed for about 30 min and magnetically stirred in the dark for 1 h to achieve adsorption-desorption equilibrium. Then, the solution was collected about 2 mL per hour and centrifuged to remove the photocatalyst. Next, the 0.22 μm of the microporous membrane were used to filter the upper suspension. The phenol concentration of the collected filter liquor was detected by a high performance liquid chromatography (HPLC) system. Chromatographic column was a Venusil XBP-C18 (4.6 × 150, Agela Technologies Inc.) column and the detection wavelength of the HPLC system was 270 nm. The mobile phase from the HPLC column consisted of water and methanol (V_{water}: $V_{methanol}$ = 45: 55), which was used for the elution and degradation of phenol. The elution time was 5 min and the flow rate was 1 mL/min. The degradation phenol process of the samples was fitted to pseudo-first-order kinetics. Thus, the rate constant *k* could be obtained from the corresponding slope of the fitting line.

2.4. Electrochemical measurement

The photocurrent response of the PDI@AuNPs were measured with 0.3 V bias voltage. A standard three electrode cell were used in the photoelectric studies. The ITO deposited with photocatalyst acted as the working electrode, a standard calomel electrode (SCE) and a platinum wire acted as reference electrode and counter electrode respectively. Na_2SO_4 (0.1 M) solution was the electrolyte solution. The working electrode of ITO/PDI@AuNPs was prepared through the dip coating method. Firstly, 5 mg PDI@AuNPs or PDI nanowire was suspended in the ethanol. Next, the slurry (5 mg/mL) prepared here was coated onto a indium-tin oxide (ITO, 2 cm × 4 cm) glass electrode and dried about 12 h. Finally, the working electrode was calcined at 100 °C for 2 h and then slowly cooled to room temperature.

The steady-state surface photovoltage (SPV) measurement system was used to measure the SPV of the materials. [33,34]A 500 W xenon lamp (CHF XQ500 W) were used to produce the monochromatic light resource. The PDI nanowire and PDI@AuNPs were tested without further treatment. The contact between the materials and the ITO electrode was non-ohmic. The resolution of spectrum was 1 nm A lock-in amplifier (SR830-DSP) with a light chopper (SR540) was applied to detect the surface photovoltage signal.

3. Results and discussion

3.1. Structure regulation of PDI@AuNPs

The morphologies of as-prepared supramolecular PDI nanowire, the AuNPs and the PDI@AuNPs were observed by the SEM, TEM (Fig. 1). The supramolecular PDI nanofibers (denoted as PDI nanowire) were prepared according the previous study. [18] Typically, the bulk PDI was dissolved in the triethylamine solution and formed the PDI solution. And then the HCl was added to the PDI solution. The PDI nanowire were formed by the hydrogen bonding and π-π stacking (Scheme 1). The diameter of the PDI nanowire was about 20 nm and the length was 100–300 nm (Fig. 1B). Next, the as-prepared AuNPs were directly viewed by the TEM. The AuNPs were uniformly dispersed, and possessed an average diameter within the range of 13 ± 1 nm without large metal nanoparticles (Fig. 1C), and the hydrate particle size distribute of the AuNPs was measured (Fig. S1A). When the AuNPs were added into the PDI solution, the AuNPs were adsorbed on the surface of the PDI (Fig. 1A and 1D). Next, the Zeta potential of AuNPs and PDI were measured to evidence the electrostatic adsorption between AuNPs and the PDI. The ξ-value of PDI changed from 4 (Fig. S1C) to −55.4 mV

(Fig. S1D) when added the AuNPs (-79.4 mV) (Fig. S1B) into the PDI solution.

Next, the XRD was used to determine the crystallinity and crystal of the PDI nanowire and different volumes of AuNPs composited with PDI (Fig. 2A). The peak at 2θ = 44.5° was owning to the crystallographic of the AuNPs (200). In addition, no significant changes in the crystal structure could be observed, which proved that the AuNPs could not change the type of self-assembled process about the supramolecular PDI. The UV–vis diffuse reflection spectra (DRS) of the PDI nanowires and PDI@AuNPs photocatalyst were shown in Fig. 2B. The PDI@AuNPs appeared a little enhanced visible light absorption than the self-assembled PDI. The band gap width of PDI changed from 1.74 eV to 1.73 eV, which was calculated according to the formula: Eg = 1240/λg (eV). The X-ray Photoelectron Spectroscopy (XPS) (Fig. S2), Fourier Transform Infrared Spectroscopy (FTIR), and Raman spectra (Fig. S3) were employed to analyse the groups, structure and components of the PDI or PDI@AuNPs in detail. The narrow spectra of C 1 s displayed at 284.26 eV, 285.62 eV, 287.29 eV and 288.65 eV (Fig. S2A), demonstrating the C=C, C—N, C—O, C=O and π-excitation. [[35]] Simultaneously, the O 1 s spectrum (Fig. S2C) exhibited three peaks at 530.78, 531.7 eV and 532.7 eV, which were attributed to C=O, C—O—C and H_2O chemistry respectively. The results of the XPS spectra had further confirmed the FTIR and Raman data. The FTIR data of PDI@AuNPs and PDI were shown at 1652 cm^{-1} C=C and 1688 cm^{-1} C=O stretching may indicate the benzene ring and carboxyl structure (Fig. S3A). The Raman spectra of PDI and PDI@AuNPs exhibited several Raman modes with frequencies of 1394 cm^{-1} and 1590 cm^{-1} (Fig. S3B). No significant changes in Raman frequency could be observed. Overall, the FTIR and Raman spectra indicating the structure of self-assemble PDI have been retained in PDI@AuNPs composite.

Again, the fluorescence emission spectra (660–850 nm) of PDI and PDI composite with different volumes of AuNPs were measured under the excitation wavelength at 650 nm (Fig. S4A). The fluorescence intensity decreased with the volumes of AuNPs increased, indicating that PDI@AuNPs reduced the combine probability of the holes and electrons. The UV–vis absorption of PDI@AuNPs shown more width range than the pure PDI (Fig. S4B), owing to the SPR effect of AuNPs. Thus AuNPs deposited on the surface of the PDI not only broaden the visible light absorption and increased the light scattering, but also reduced the combine probability of the electron-hole pairs.

3.2. SPR effect enhance the photocatalytic activity

The photocatalytic activity of the samples prepared here were evaluated by the oxidation of phenol. Firstly, a series of experiments were performed to explore the optimized conditions for synthesizing PDI@AuNPs. As is depicted (Figs. 3 and S5), different kinds of conditions (volumes of AuNPs and HCl, time and temperature) of the self-assembled process were be studied to confirm the optimum preparation conditions. The changes of the phenol concentration under visible light (λ > 420 nm) was used to evaluate the photocatalytic activity of the different catalysts. As shown in the Figs. 3 and S5, the mass ratio of m (PDI): m (AuNPs) = 14.35, the volume of HCl (4 M) was 13 ml, the self-assembled time was 3 h at room temperature served as the final condition for the synthesis of PDI@AuNPs, which degrade about 85% of phenol (5 ppm) during 6 h (Fig. 3C) and the degradation rate constants *k* reached 0.307 h^{-1} (Fig. 3D).

The PDI@AuNPs exhibited higher visible photocatalytic activity than the pure PDI nanowire or AuNPs (Fig. 4A). The degradation phenol process was fitted to the pseudo-first-order kinetics. Therefore, the rate constant (*k*) could be obtained from the corresponding slope of the fitting line (Fig. 4B). The photocatalytic activity of PDI@AuNPs reached the maximum value of 0.307 h^{-1}, which is about 1.72 times higher than the pure PDI nanowire (0.179 h^{-1}). Most importantly, the new catalyst PDI@AuNPs exhibits superior photodegradation performance compared with other reported visible-light active photocatalysts
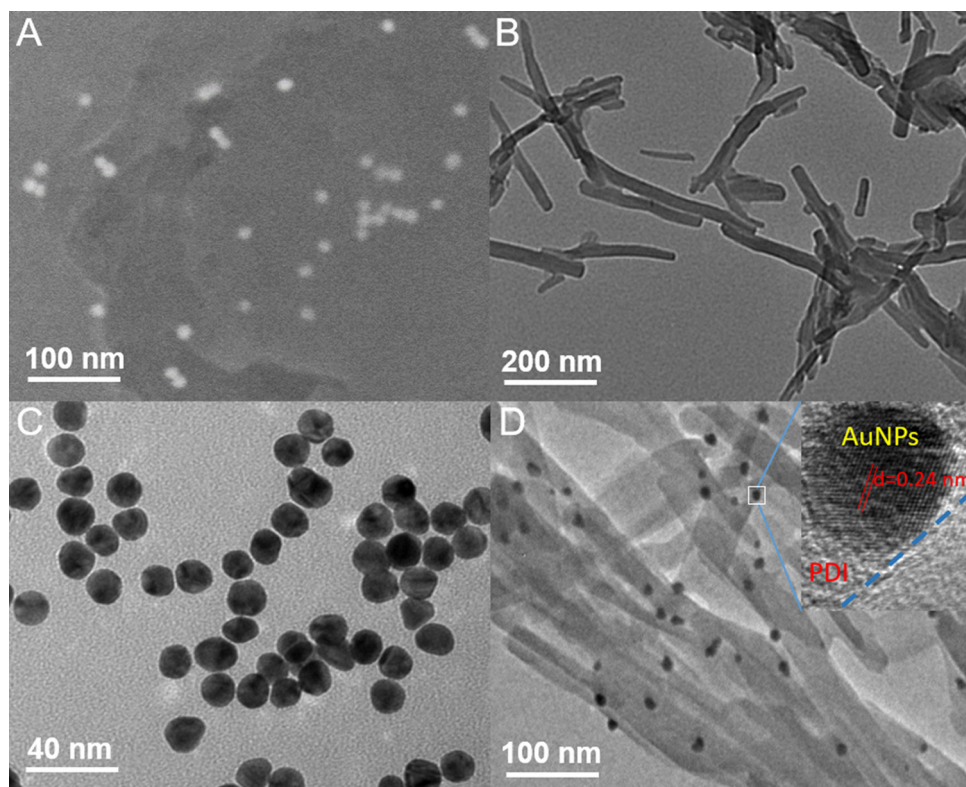
Fig. 1. (A) SEM images of PDI@AuNPs; TEM images of (B) self-assembled PDI; (C) AuNPs; (D) HR-TEM images of PDI@AuNPs.
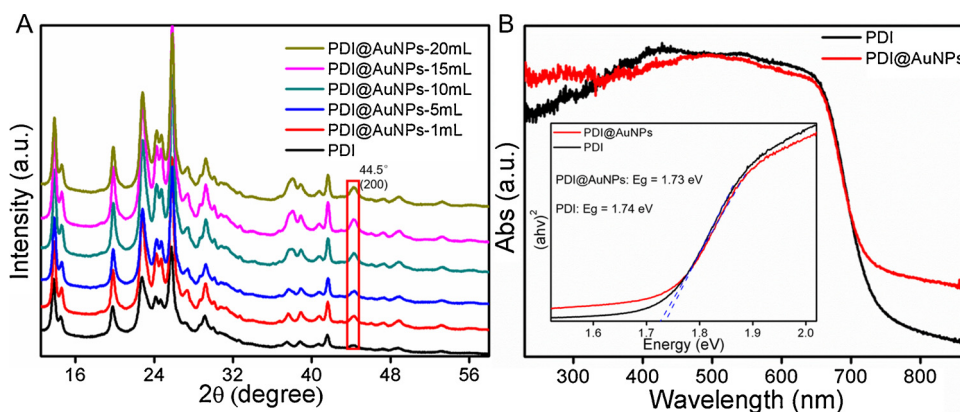

Fig. 2. (A) A series of samples XRD spectra; (B) The UV–vis diffuse reflection spectra (DRS) of self-assembled PDI and PDI@AuNPs photocatalyst. Inset: The bandgap width of PDI and PDI@AuNPs.

such as g-C$_3$N$_4$, [[36]]] Bulk PDI, and Bi$_2$WO$_6$ [[37]]. The activity of the PDI@AuNPs is 17, 4.4, 10.2 times higher than the g-C$_3$N$_4$, Bulk PDI, Bi$_2$WO$_6$ respectively (Fig. 4A). The results (Fig. S6) were recorded by HPLC system with an ultraviolet-visible detector. The peak located at 3.57 min corresponds to phenol, and the other peaks of 1.93 min, 2.50 min and 2.87 min correspond to Hydroquinol, p-benzoquinone and Bi-phenol respectively.[17] The new catalyst PDI@AuNPs system also proved to be photoactive in the degradation of 2, 4-Dichlorophenol and bisphenol A, as shown in Fig. S7. In order to evaluate the catalytic stability, a three-cycle test of PDI and PDI@AuNPs (Fig. 4C) catalyst degradation of phenol were studied. Compared with the pure PDI, the activity of PDI@AuNPs remained great stability. On the contrary, the activity of pure PDI decreased about 50% at the third cycle. Thus the PDI@AuNPs could be efficiently recycled than PDI nanowire in neutral environment (pH = 7). The recycling test in the acid (pH = 5.6) and alkaline (pH = 9.3) environment also have been investigated to explore the stability of the PDI@AuNPs (Fig. 4D). The results showed that the

stability of the composite catalyst in the acid environment is higher than the PDI@AuNPs in the neutral (pH = 7) and alkaline (pH = 9.3). The loss of activity at neutral solution could be attributed to the de-polymerization of PDI and the absorption between the PDI with AuNPs during the photodegradation of organic pollutants [18,20,38]. Furthermore, the results of wavelength-dependent photodegradation showed that the photodegradation rate constant (*k*) was related to optical absorption as a function of wavelength (Fig. S8). Owing to the SPR excitation of AuNPs, the PDI@AuNPs exhibited higher photo-catalytic activity under 500 nm. The results indicated that the performance in photodegradation of PDI@AuNPs may rely on the optical absorption.

3.3. Mechanism of the SPR effect enhance catalytic activity

The photoelectrochemistry process was used to study the mechanism of enhanced photocatalytic activity of PDI@AuNPs composite.
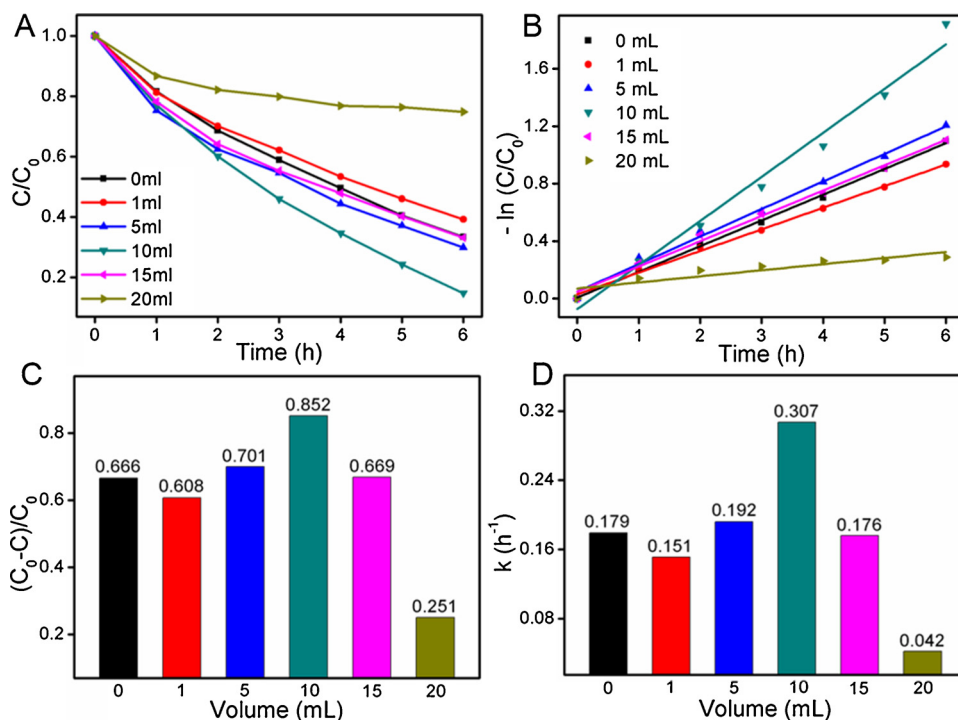
Fig. 3. (A) Photocatalytic degradation of 5 ppm phenol under visible light (λ > 420 nm); (B) The first order kinetics curve fitting of samples degradation phenol; (C) The degradation rate of samples degradation phenol about 6 h; (D) The degradation rate constants k of samples degradation phenol.

The separation of photogenerated electron-hole play a very important role in the photocatalytic degradation of organic pollutants process. In this work, the carrier separation efficiency of photocatalyst were further studied by some effective techniques such as photocurrent test, surface photovoltage spectroscopy (SPV) and cyclic voltammetry (Fig. 5). The stable photocurrent response of the PDI@AuNPs composite was higher than self-assembled PDI nanowire (Fig. 5A) under the visible light (> 420 nm) irradiation. The enhanced photocurrent

response of the PDI@AuNPs proved that the separation efficiency of photogenerated carriers and the photocatalytic performance are improved. Similarly, the photovoltaic response intensity (Fig. 5B) and cyclic voltammetry spectra (Fig. 5C) of PDI@AuNPs were higher than that of pure PDI. Therefore, the higher photocurrent, photovoltaic response intensity revealed that the PDI@AuNPs has a higher carrier separation efficiency than the PDI nanowire, which could be owing to the higher π electrons delocalization and SPR excitation in the
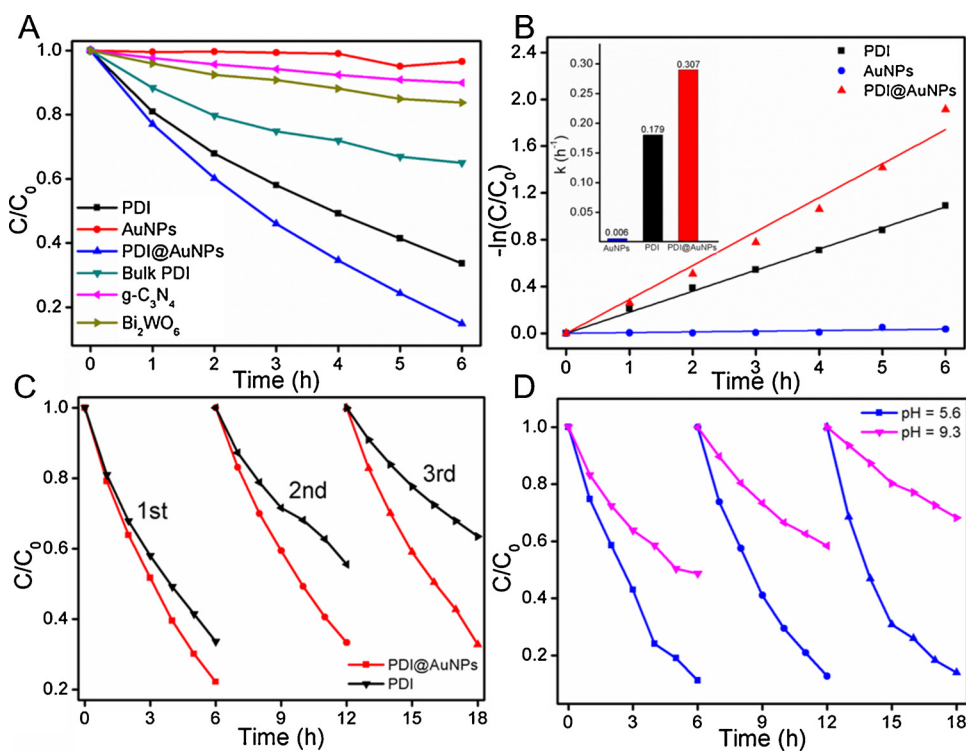

Fig. 4. (A) The degradation plot of phenol in the presence of AuNPs, PDI, PDI@AuNPs and other catalyst (Bulk PDI, g-C₃N₄, Bi₂WO₆, PTCDI) under visible light (λ > 420 nm); (B) The first order kinetics curve fitting of degradation phenol in the presence of AuNPs, PDI and PDI@AuNPs; (C) PDI and PDI@AuNPs cycle degradation of phenol performance test in the neutral environment; (D) PDI@AuNPs cycle degradation of phenol performance test in the acid (pH = 5.6) and alkaline (pH = 9.3) environment.
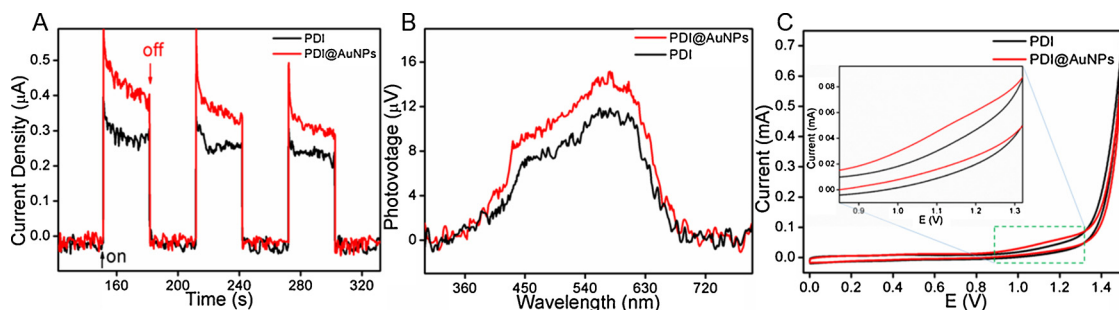
Fig. 5. Photocurrent response curves (A), surface photovoltage spectroscopy (B) and cyclic voltammetry spectra (C) of PDI and PDI@AuNPs.
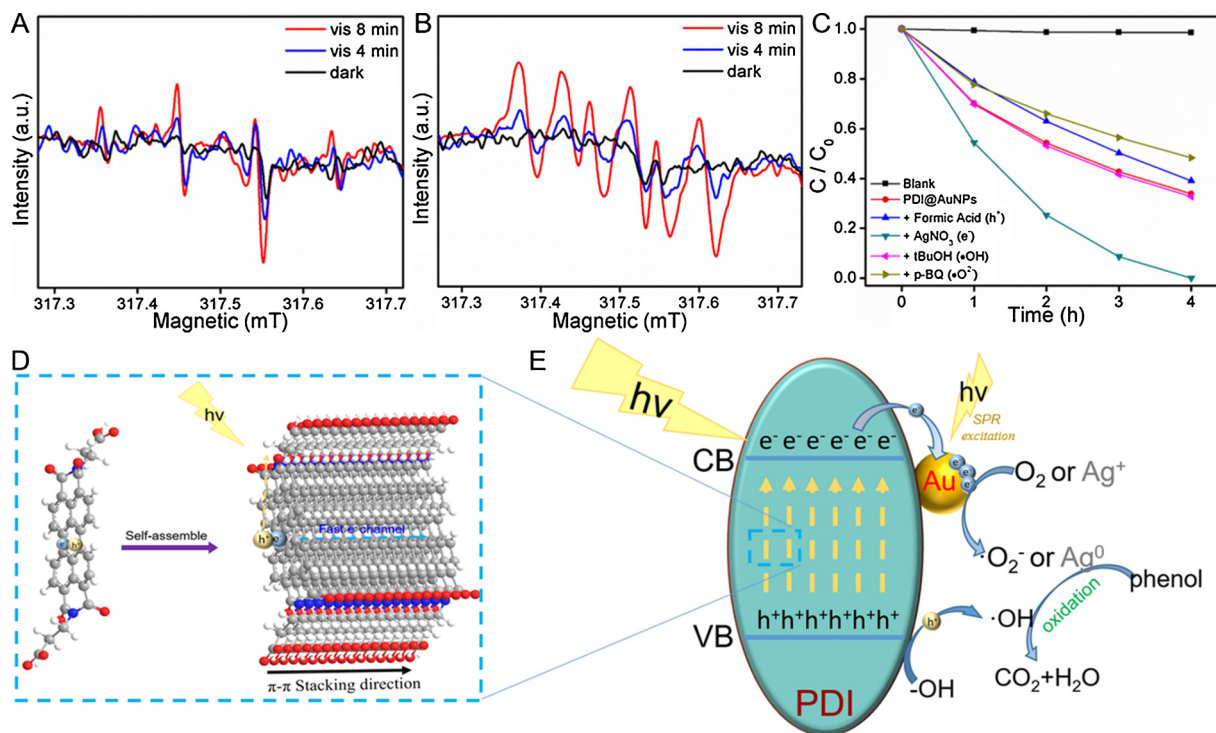

Fig. 6. Electron paramagnetic resonance (ESR) spectra of PDI@AuNPs in water detected ·OH (A) and DMSO solvebts detected ·O_2^- (B); (C) Plots of photogenerated carriers trapping in the system of photodegradation of phenol by PDI@AuNPs. (D) Mechanism of charges separation of self-assembled PDI. (E) Schematic description of the mechanism for the photocatalytic oxidation of phenol on PDI@AuNPs photocatalyst.

PDI@AuNPs surface.

Subsequently, the specific active species of PDI@AuNPs composite in the photocatalytic degradation reaction were revealed by the electron spin resonance (ESR) tests and trapping experiments. The signal responses of the hydroxyl radical (·OH) (Fig. 6A) and superoxide radical (·O_2^-) (Fig. 6B) were both detected by the ESR spectrometer. The DMPO (5,5-dimethyl-1-pyrroline Noxide) acted as a spin trap could reflect the presence of ·OH or ·O_2^- capably. It could be observed that both the ·O_2^- and ·OH appeared during the photocatalytic process. Concretely, the ·O_2^- had a stronger signal response than that of the · OH under visible light irradiation. The results of Fig. 6C showed the photodegradation tests of phenol with the addition of holes scavenger (formic acid), superoxide radical scavenger (p-benzoquinone, p-BQ), electrons scavenger (AgNO₃) and hydroxyl radical scavenger (t-BuOH) under visible light irradiation, respectively. Overall, the results of trapping experiments showed agreement with that of ESR tests. The results indicated that the superoxide radical (·O_2^-) were the main active species in photocatalytic process of PDI@AuNPs.

Based on the discussion above, a schematic description of the mechanism for the photocatalytic degradation pollutants process of the PDI@AuNPs is proposed in Fig. 6E. Specifically speaking, the PDI

(Fig. 6D) and the AuNPs generated the electrons and holes when the visible light irradiate the PDI@AuNPs. The electromagnetic filed mediated plasmonic of AuNPs could take the form of a resonance energy transfer (RET) process. [20,24,39] Thus, the RET process and SPR effect are beneficial for utilizing the visible light. On the other hand, the fermi level of Au (0.45 eV, versus NHE) [40] is lower than the conduction band (CB) edge of PDI nanowire (−0.17 eV, versus NHE) [18]. Thus, the AuNPs deposited on the PDI surface may act as the electron sinks and retard the recombination of the photogenerated electrons-hole from the PDI nanowire. At the same time, the ·O_2^- could be formed by photogenerated electrons transferred on the surface of AuNPs. Meanwhile, the ·OH is generated via the reaction of −OH and the photogenerated holes on the surface of the PDI. [41] The interaction of the photogenerated holes and ·OH with the reactive oxidized intermediate initiate a series of oxidation reactions. Therefore, the RET process and SPR effect of AuNPs are beneficial for utilizing the visible light and transferring the photogenerated holes and electrons, which was responsible for the highly efficient photocatalytic degradation of pollutants.

4. Conclusion

In this work, the SPR-supported visible-light-responsive photocatalyst of PDI@AuNPs were prepared through the electrostatic adsorption. The SPR effect of the AuNPs and the RET process could be effectively used for improving the visible light absorption. On the other hand, the photogenerated electrons from the PDI nanowire could transferred to the surface of the AuNPs and formed the $\cdot O_2^-$ fleetly. Meanwhile, the photogenerated holes at the PDI could reacted with the $-OH$. In summary, we have reported a strategy via SPR effect of AuNPs for enhancing the photocatalytic performance and stability of PDI nanowire, which is expected to provide a facile guideline for improving the catalytic activity of organic photocatalysts.

Acknowledgements

Appendix A. Supplementary data

Supplementary material related to this article can be found, in the online version, at doi:https://doi.org/10.1016/j.apcatb.2018.08.009.

References

[1] M.A. Fox, M.T. Dulay, Heterogeneous photocatalysis, Chem. Rev. 93 (1993) 341–357.

[2] J. Ryu, W. Choi, Substrate-specific photocatalytic activities of TiO_2 and multi-activity test for water treatment application, Environ. Sci. Technol. 42 (2008) 294–300.

[3] A. Fujishima, Electrochemical photolysis of water at a semiconductor electrode, Nature 238 (1972) 37–38.

[4] F. Cao, Y. Li, C. Tang, Fast synthesis of anatase TiO_2 single crystals by a facile solid-state method, Res. Chem. Intermed. 42 (2016) 5975–5981.

[5] Z. Bian, J. Zhu, H. Li, Solvothermal alcoholysis synthesis of hierarchical TiO_2 with enhanced activity in environmental and energy photocatalysis, J. Photochem. Photobiol. C Photochem. Rev. 28 (2016) 72–86.

[6] C. Tang, L. Liu, Y. Li, Aerosol spray assisted assembly of TiO_2 mesocrystals into hierarchical hollow microspheres with enhanced photocatalytic performance, Appl. Catal. B: Environ. 201 (2017) 41–47.

[7] Y. Li, Y. Bian, H. Qin, Photocatalytic reduction behavior of hexavalent chromium on hydroxyl modified titanium dioxide, Appl. Catal. B: Environ. 206 (2017) 293–299.

[8] H. Qin, Y. Bian, Y. Zhang, Effect of Ti (III) surface defects on the process of photocatalytic reduction of hexavalent chromium, Chin. J. Chem. 35 (2017) 203–208.

[9] C.M. Ronconi, C. Ribeiro, L.O.S. Bulhoes, E.C. Pereira, Insights for phase control in TiO_2 nanoparticles from polymeric precursors method, J. Alloys 466 (2008) 435–438.

[10] L.Y. Wang, Y.P. Sun, B.S. Xu, Comparison study on the size and phase control of nanocrystalline TiO_2 in three Ti–Si oxide structures, J. Mater. Sci. 43 (2008) 1979–1986.

[11] D.S. Wang, N.H. Lee, D.Y. Lee, J.S. Song, S.H. Shin, S.J. Kim, Phase transition control of nanostructured TiO_2 powders with additions of various metal chlorides, Smart Mater. Struct. 15 (2006) 74–80.

[12] A. Testino, I.R. Bellobono, V. Buscaglia, C. Canevali, M.S.Polizzi D'Arienzo, R. Scotti, F. Morazzoni, Optimizing the photocatalytic properties of hydrothermal TiO_2 by the control of phase composition and particle morphology. A systematic approach, J. Am. Chem. Soc. 129 (2007) 3564–3575.

[13] H.P. Xu, Y.P. Sun, J.W. Wang, H.Q. Zhan, X.M. Chen, Control of particle size and crystal phase of TiO_2 nanocrystalline prepared by HF-PCVD, Rare Metal Mater. Eng. 34 (2005) 1089–1093.

[14] M.A. Frank, C. Meltzer, B. Braunschweig, Functionalization of steel surfaces with organic acids: influence on wetting and corrosion behavior, Appl. Surf. Sci. 404 (2017) 326–333.

[15] A. Datar, K. Balakrishnan, L. Zang, One-dimensional self-assembly of a water soluble perylene diimide molecule by pH triggered hydrogelation, Chem. Commun. (Camb.) 49 (2013) 6894–6896.

[16] C. Shuai, P. Slattum, C. Wang, Self-assembly of perylene imide molecules into 1D nanostructures: methods, morphologies, and applications, Chem. Rev. 115 (2015) 11967–11998.

[17] D. Liu, J. Wang, X. Bai, Self-assembled PDINH supramolecular system for photocatalysis under visible light, Adv. Mater. 28 (2016) 7284–7290.

[18] J. Wang, W. Shi, D. Liu, Supramolecular organic nanofibers with highly efficient and stable visible light photooxidation performance, Appl. Catal. B: Environ. 202 (2017) 289–297.

[19] L. Zeng, T. Liu, C. He, Organized aggregation makes insoluble perylene diimide efficient for the reduction of aryl halides via consecutive visible light-induced electron-transfer processes, J. Am. Chem. Soc. 138 (2016) 3958–3961.

[20] F. Lin, B. Shao, Z. Li, J.Y. Zhang, H. Wang, S.H. Zhang, M. Hartuta, J.H. Huang, Visible light photocatalysis over solid acid: enhanced by gold plasmonic effect, Appl. Catal. B: Environ. 218 (2017) 480–487.

[21] S.K. Cushing, J.T. Li, F.K. Meng, T.R. Senty, S. Suri, M.J. Zhi, M. Li, A.D. Bristow, N.Q. Wu, Photocatalytic activity enhanced by plasmonic resonant energy transfer from metal to semiconductor, J. Am. Chem. Soc. 134 (2012) 15033–15041.

[22] K. Awazu, M. Fujimaki, C. Rockstuhl, J. Tominaga, H. Murakami, Y. Ohki, N. Yoshida, T. Watanabe, A plasmonic photocatalyst consisting of silver nanoparticles embedded in titanium dioxide, J. Am. Chem. Soc. 130 (2008) 1676–1680.

[23] C. Hu, T. Peng, X. Hu, Y. Nie, X. Zhou, J. Qu, H. He, Plasmon-induced photodegradation of toxic pollutants with $Ag-AgI/Al_2O_3$ under visible-light irradiation, J. Am. Chem. Soc. 132 (2010) 857–862.

[24] H. Yuzawa, T. Yoshida, H. Yoshida, Gold nanoparticles on titanium oxide effective for photocatalytic hydrogen formation under visible light, Appl. Catal. B: Environ. 115–116 (2012) 294–302.

[25] H. Yuzawa, H. Yoshid, Direct aromatic-ring amination by aqueous ammonia with a platinum loaded titanium oxide photocatalyst, Chem. Commun. 46 (2010) 8854–8856.

[26] Q. Zhang, D.Q. Lima, I. Lee, F. Zaera, M. Chi, Y. Li, A highly active titanium dioxide based visible-light photocatalyst with nonmetal doping and plasmonic metal decoration, Angew. Chem. Int. Ed. 123 (2011) 7226–7230.

[27] S. Naya, A. Inoue, H. Tada, Self-assembled heterosupramolecular visible light photocatalyst consisting of gold nanoparticle-loaded titanium (IV) dioxide and surfactant, J. Am. Chem. Soc. 132 (2010) 6292–6293.

[28] Z. Liu, W. Hou, P. Pavaskar, M. Aykol, S.B. Cronin, Plasmon resonant enhancement of photocatalytic water splitting under visible illumination, Nano Lett. 11 (2011) 1111–1116.

[29] D.B. Ingram, S. Linic, Water splitting on composite plasmonic-metal/semiconductor photoelectrodes: evidence for selective plasmon-induced formation of charge carriers near the semiconductor surface, J. Am. Chem. Soc. 133 (2011) 5202–5205.

[30] I. Thomann, B.A. Pinaud, Z. Chen, B.M. Clemens, T.F. Jaramillo, M.L. Brongersma, Plasmon enhanced solar-to-fuel energy conversion, Nano Lett. 11 (2011) 3440–3446.

[31] K. Zhang, J. Wang, W.J. Jiang, W.Q. Yao, H.P. Yang, Y.F. Zhu, Self-assembled perylene diimide based supramolecular heterojunction with Bi_2WO_6 for efficient visible-light-driven photocatalysis, Appl. Catal. B: Environ. 232 (2018) 175–181.

[32] D. Zhong, K.C. Yang, Y.Y. Wang, X.M. Yang, Dual-channel sensing strategy based on gold nanoparticles cooperating with carbon dots and hairpin structure for assaying RNA and DNA, Talanta 175 (2017) 217–233.

[33] H. Fan, H. Li, B. Liu, Y. Lu, T. Xie, D. Wang, Photoinduced charge transfer properties and photocatalytic activity in $Bi_2O_3/BaTiO_3$ Composite Photocatalyst, ACS Appl. Mater. Interfaces 2 (2014) 4853–4857.

[34] Z. Wei, J.S. Hu, K.J. Zhu, W.Q. Wei, X.G. Ma, Y.F. Zhu, Self-assembled polymer phenylethnylcopper nanowires for photoelectrochemical and photocatalytic performance under visible light, Appl. Catal. B: Environ. 226 (2018) 616–623.

[35] Y. Li, M.C. Zhang, X.H. Guo, R. Wen, X. Li, X.F. Li, S.J. Li, L.J. Ma, Growth of high-quality covalent organic framework nanosheets at the interface of two miscible organic solvents, Nanoscale Horiz. 3 (2018) 205–212.

[36] M. Zhang, W.Q. Yao, Y.H. Lv, X.J. Bai, Y.F. Liu, W.J. Jiang, Y.F. Zhu, Enhancement of mineralization ability of C_3N_4 via a lower valence position by a tetra-cyanoquinodimethane organic semiconductor, J. Mater. Chem. A Mater. Energy Sustain. 2 (2014) 11432–11438.

[37] C. Zhang, Y.F. Zhu, Synthesis of square Bi_2WO_6 nanoplates as high-activity visible-light-Driven photocatalysts, Chem. Mater. 17 (2005) 3537–3545.

[38] B. Weng, K.Q. Lu, Z. Tang, H.M. Chen, Y.J. Xu, Stabilizing ultrasmall Au clusters for enhanced photoredox catalysis, Nat. Commun. 9 (2018) 1543.

[39] F. Lin, Y.N. Zhang, L. Wang, Y.L. Zhang, D.E. Wang, M. Yang, J.H. Yang, B.Y. Zhang, Z.X. Jiang, C. Li, Highly efficient photocatalytic oxidation of sulfur-containing organic compounds and dyes on TiO_2 with dual cocatalysts Pt and RuO_2, Appl. Catal. B: Environ. 127 (2012) 363–370.

[40] V. Subramanian, E.E. Wolf, P.V. Kamat, Catalysis with TiO_2/Gold Nanocomposites. Effect of metal particle size on the fermi level equilibration, J. Am. Chem. Soc. 126 (2004) 4943–4950.

[41] M.A. Fox, A.A. Abdel-wahab, Selectivity in the TiO_2-mediated photocatalytic oxidation of thioethers, Tetrahedron Lett. 31 (1990) 4533–4536.